Cryo-EM and cellular dissection uncover versatile PME-1 activities in PP2A holoenzyme demethylation and inhibition

Yongna Xing (xing@oncology.wisc.edu)
University of Wisconsin-Madison https://orcid.org/0000-0002-9834-528X
Yitong Li
Department of Oncology at University of Wisconsin-Madison
Michael Rowse
University of Wisconsin Madison
Cheng-Guo Wu
Biophysics program at University of Wisconsin-Madison
Anastasia Bravos
University of Wisconsin Madison
Ylva Ivarsson
Uppsala University
Stefan Strack
University of Iowa https://orcid.org/0000-0002-6175-7280

Article

Keywords: Biochemical Dissections, Disordered Motifs, Multiple Dynamic Structured Contacts, Methylesterase Activation, AKT-p53 Signaling

Posted Date: May 3rd, 2021

DOI: https://doi.org/10.21203/rs.3.rs-372534/v1

Abstract

Protein phosphatase 2A (PP2A) methylesterase 1 (PME-1) is cancer-promoting but essential for development, and long-believed to remove carboxymethylation, a central modification, from the common PP2A core enzyme but not diverse holoenzymes that target broad cellular signaling by recognizing specific disordered motifs via regulatory subunits. On the contrary, our biochemical dissection and high-resolution cryo-EM structural analysis of a PP2A-B' holoenzyme-PME-1 complex reveal that PME-1 disordered motifs, including phosphatase substrate-mimicking motifs, tether to the holoenzyme at remote sites, block its substrate binding, and allow large structural shifts in both holoenzyme and PME-1 to enable multiptle dynamic structured contacts and induce methylesterase activation toward the holoenzyme. PME-1 inhibitor and B'-interface mutations differentially modulate cellular PP2A methylation and allow us to uncover cellular PME-1 functions in AKT-p53 signaling. Our studies demonstrate how dynamic structured cores and disordered motifs create versatile activities and lay a foundation for investigating and targeting multifaceted activities toward broad PP2A complexes in cellular signaling.

Introduction

Protein phosphatase 2A (PP2A) is a major and the most abundant serine/threonine phosphatase in mammalian cells and dephosphorylates ~half cellular proteins[1-3]. The cellular functions of PP2A rely on the formation of structurally distinct diverse heterotrimeric holoenzymes[4-6]. Each holoenzyme consists of a dimeric core enzyme formed by the scaffolding A and catalytic C (C or PP2Ac) subunits and a diverse regulatory subunit. The regulatory subunits belong to four major families (B/B55/PR55, B'/B56/PR61, B"/PR72, and B"'/Striatin), and dictate specific substrate recognition[7-9]. Recent studies arrive at a merging theme that PP2A holoenzymes recognize substrates by binding to short linear motifs (SLiMs) in substrates[10-13]. PP2A holoenzymes are highly regulated by carboxymethylation of the PP2Ac tail, which is reversibly controlled by two highly conserved enzymes, PP2A-specific leucine carboxyl methyltransferase (LCMT-1)[14,15] and methylesterase (PME-1)[16]. Methylation facilitates the assembly of stable heterotrimeric holoenzymes in cells[17,18]. Dysregulation of PP2A holoenzymes or altered holoenzyme functions causes many human diseases, including cancer, heart diseases, and neurodegenerative disorders[19,20]. Consistently, LCMT-1 is essential for cell survival[21], and deletion of PME-1 in mice is perinatally lethal[22].

Many layers of structural mechanisms strictly control LCMT-1/PME-1's activities for proper PP2A holoenzyme homeostasis. Both enzymes are unique in their deep substrate-binding pockets and have low sequence similarity to other methyl-transferases/esterases[15,16,23,24]. Although they catalyze reactions on the PP2Ac tail, "RPDYFL", they are inactive toward the corresponding synthetic peptides[23-25]. Activation of their enzymatic activities rely on binding to the phosphatase active site, which induces significant changes in LCMT-1 to accommodate the tail[24] and global conformational changes in PME-1 to create substrate-binding pocket and rearrange catalytic triads into active configuration[23]. Furthermore, LCMT-1 activity is enhanced by the A-subunit and phosphatase activation, making it highly selective toward the

active core enzyme[24,26]. The tight control of PP2A methylation helps maintain PP2A in either latent inactive or active substrate-specific forms.

PME-1 was thought to also act on the PP2A core enzyme and downregulate holoenzyme assembly. Many lines of evidence support this long-term belief. First, PP2A holoenzymes are predominately methylated in cells[18,27,28], and themal dynamically the most stable forms with nanomolar intersubunit binding affinities[29]. In contrast, PP2A interacts with dynamic regulatory proteins with micromolar binding affinities, such as LCMT-1 and PME-1 above and TIPRL (TOR signaling pathway regulator-like)/a4 as detailed below. Structural overlay of PP2A holoenzymes[30-32] and the PP2A core enzyme-PME-1 complex[23] indicates that PP2A regulatory subunits would hinder PME-1 binding and prevent it from acting on holoenzymes (Fig.1a). A recent striking discovery, however, starts to question the static view on cellular holoenzyme stability and PME-1 activity. TIPRL selectively attacks the malleable phosphotaase active site of unmethylated PP2A, allowing a4 to unfold PP2Ac into a partially folded latent form, by which TIPRL/a4 readily disassemble the unmethylated PP2A holoenzymes[33,34]. This observation raises the possibility that the predominate methylated PP2A holoenzymes observed in cells is the result of dissociation of unmethylated holoenzymes.

Could PME-1 demethylate PP2A holoenzymes? The highly malleable enzyme core and long disordered motifs in PME-1 intrigued us to test this notion. Here we demonstrate the ability of PME-1 to interact with and demethylate PP2A holoenzymes and the function of PME-1 disordered motifs and holoenzyme substrate-mimicking SLiM. The high-resolution cryo-EM structure of a PP2A-B' holoenzyme-PME-1 complex reveals that PME-1 disordered motifs tether to the holoenzyme, blocking substrate-binding and allowing large structural shifts in both holoenzyme and PME-1 to accommodate multipartite structured core interactions and induce methylesterase activation. PME-1 inhibitor and PME-1-B' interface mutations allow us to dissect novel PME-1 activities in cellular AKT-p53 signaling.

Results

PME-1 interacts with PP2A-B' holoenzymes and induces a more open holoenzyme conformation

Alignment of high-resolution crystal structures of PP2A holoenzymes and the PP2A core enzyme-PME-1 complex shows that PP2A regulatory subunits in holoenzymes exert a huge steric hindrance that would exclude PME-1 binding (Fig. 1a, PP2A-B'g1 holoenzyme shown). Contradictory to this structural prediction, PME-1 co-migrates readily well with the PP2A-B'e holoenzyme (Fig. 1b), demonstrating a stable PME-1-PP2A holoenzyme interaction and the necessity of large conformational changes. We probed the holoenzyme conformation using an A-subunit FRET (fluorescence resonance energy transfer) sensor[30], in which TC-FLASH produced by tetracysteine peptide (TC) fused to the C-terminus serves as an acceptor for the CFP (cyan fluorescent protein) fused to the N-terminus. Using the core enzyme and PP2A-B'g1 holoenzyme containing this FRET sensor, we showed that the energy transfer efficiency in the holoenzyme is much higher than the core enzyme, but significantly reduced upon the addition of PME-1 (Fig. 1c). This data demonstrates a much tighter holoenzyme conformation, corroborating the previous

observation[30], and indicates that PME-1 can interact with the holoenzyme and induce a more open holoenzyme conformation.

We next validated the interactions between PME-1 and PP2A-B' holoenzymes in mammalian cells. We co-expressed PME-1-mRuby fusion protein and recombinant B' regulatory subunits harboring HA-tag and assessed their interactions by co-immunoprecipitation (co-IP). PME-1-mRuby readily interacts with PP2Ac and multiple HA-tagged regulatory subunits in the B' family, B'b, B'g1, B'g3, and B'd (Fig. 1d), suggesting that PME-1 might interact with the conserved common core in B' subunits (Extended Data Fig. 1a). This common core is also crucial for substrate recognition [10-13]. Compared to other B' family members, B'd interacts with a much higher ratio of PP2Ac over PME-1 (Fig. 1d), suggesting that the interaction between PME-1 and the PP2A-B'd holoenzyme might be reduced by other structural elements unique in B'd (Extended Data Fig. 1a). Consistently, a much lower stoichiometric amount of PME-1 co-migrates with the PP2A- B'd holoenzyme over gel filtration chromatography (Extended Data Fig. 1b). These data support that PME-1 interacts with different B' subunits in cells, and unique structural elements outside the common core might modulate this interaction.

PME-1 catalyzes direct demethylation of three families of PP2A holoenzymes

PME-1 activation relies on its binding to the PP2A active site[23]. The holoenzyme conformational changes induced by PME-1 might alleviate steric hindrance and allow PME-1 to interact with the PP2A active site, leading to methylesterase activation toward holoenzymes. To test this hypothesis, we assembled the core enzyme and three representative PP2A holoenzymes from three families using Bα, B'γ1 and PR70 with higher than 90% *in vitro* methylation. After incubation with PME-1, the methylation level of all three holoenzymes decreases significantly, comparable to that of the core enzyme (Fig. 1e). Our results suggest that PME-1-PP2A holoenzyme interactions enable all sequential events needed for PME-1 activation, allowing PME-1 to demethylate PP2A holoenzymes directly.

Mapping of B'-binding motifs in PME-1

The ability of PME-1 to induce conformational changes in PP2A holoenzyme led us to search for additional contacts made by PME-1 prior to its interaction with the PP2A active site. PME-1 has two ~40-residue disordered regions at the N-terminus and internal loop (Fig. 2a). The latter harbors a SLiM (^{251}VEGII^{256}E) highly similar to B' substrates that interact with the conserved B' common core via a signature motif "LxxIxE"[10-13]. Consistent with this observation, full-length PME-1 (PME-1 FL) interacts readily well with B'g1 as demonstrated using isothermal titration calorimetry (ITC) (Fig. 2b). The deletion of the internal loop harboring the B'-SLiM (ΔIL) abolishes their interaction completely (Fig. 2b). Intriguingly, deletion of N-terminal 18 residues (ΔN18) reduces the binding affinity by ~8 fold (Fig. 2b). To demonstrate that these PME-1 disordered regions contribute to holoenzyme interactions, we showed that, while PME-1 FL co-migrates readily well with the PP2A-B'g1 holoenzyme over gel filtration chromatography (Fig. 2c, left), both PME-1 truncations, ΔIL and ΔN18, drastically decreased PME-1 interaction with the PP2A-B'g1 holoenzyme (Fig. 2c, middle and right).

Together with dual interactions of the PME-1 core to the PP2A active site and PP2Ac-tail[23], these results indicate that PME-1 makes multi-partite interactions with PP2A-B' holoenzymes. The direct interactions between PME-1 disordered motifs and PP2A regulatory subunit are essential for stable interactions with the PP2A holoenzyme.

PME-1 inhibits substrate recognition by PP2A holoenzyme

Since the B'-binding motif in the PME-1 internal loop is similar to those in substrates (Fig. 2a), we examined the potential role of PME-1 in blocking substrate recognition by PP2A holoenzymes. Previously we elucidated the SLiM-based interactions that target PP2A-B' to its substrates using proteomic peptide phage display (ProP-PD)[10]. In parallel, we also performed ProP-PD for the holoenzyme in complex with PME-1. The presence of PME-1 blocked the binding of all peptide motifs recognized by the PP2A-B'g1 holoenzyme, and reduced the counts for all B'-binding motifs to zero in phage selection (Extended Data Fig. 2a). SYT16 peptide was the strongest hits of B' substrates identified by ProP-PD[10]. By competition pull-down assay, we showed that the interaction between GST-SYT16 and PP2A-B'γ1 was blocked by increasing concentrations of PME-1 (Fig. 3b). No competitions were detected between PME-1 ΔIL or PME-1 ΔN18 and the PP2A-B'γ1 substrate (Fig 3b). Our data demonstrated that PME-1 is capable of blocking substrate recognition of the holoenzyme, which relies on PME-1-holoenzyme interactions and the substrate-mimicking SLiM in PME-1 (Extended Data Fig. 2b).

Overall structure of the PP2A-B'g1-PME-1 complex

To define the structural and molecular basis that enables PME-1 to interact with and demethylate PP2A holoenzymes and dissect its multifaceted activities, we determined a three-dimensional structure of the PP2A-B'g1-PME-1 heterotetrameric complex using single-particle cryoelectron microscopy (cryo-EM). To trap the enzymatic intermediate, we assembled the complex using the fully methylated PP2A-B'g1 holoenzyme and an inactive PME-1 mutant, S156A[23], followed by covalent crosslink by glutaraldehyde. After extensive 2D and 3D classifications and careful separation of the tetrameric complex particles from the unbound holoenzyme, the structure was finally determined at an overall resolution of 3.4 Å (Extended Data Fig. 3, Table 1). The PP2A-B'g1-PME-1 complex adopts a pentagram architecture with a size of 100 x 100 x 90 Å (Fig. 3a). The structure reveals multiple B'-PME-1 interfaces, large conformational changes in both the holoenzyme and PME-1, and orchestrated mechanisms for PME-1's multifaceted activities.

The PME-1-bound holoenzyme has a similar overall architecture and maintains most intersubunit interfaces but exhibits three major structural changes compared to the unbound holoenzyme. Overlaying structures by PP2Ac showed that the last five huntingtin-elongation-A-subunit-TOR (HEAT) repeats of the A-subunit remains mostly unchanged. The N-terminal ten HEAT repeats shift significantly by increasing distances of 4 to 12 Å from HEAT repeat ten to one, resulting in a 12 Å shift in B' that alleviates the steric hindrance for PME-1 binding (Fig. 3b). This structural observation is consistent with the sigal changes in the holoenzyme FRET sensor in response to PME-1 binding (Fig. 1c). Finally, the methylated PP2Ac tail has a drastically reduced occupancy to the A-B' interface compared to the holoenzyme as detailed later.

PME-1-binding largely suppresses the holoenzyme activities. In addition to the direct binding and blocking of the phosphatase active site, PME-1 also occupies the B' protein groove for recruiting substrates. PME-1 undergoes a significant angular movement away from B' up to 6 Å pivoted at the PME-1 helix contacting the phosphatase active site (Fig. 3c). The later remains the same compared to the core enzyme-PME-1 complex (Fig. 3c). The PME-1 angular shift further accommodates B'-PME-1 interactions. This changes is different from the global allosteric changes essential for methylesterase activation, underscoring the ability of PME-1 to undergo different modes of dynamic changes.

B'-PME-1 interfaces

Three separate interfaces involving both PME-1 structured core and disordered regions govern the interactions with B'g1 (Fig. 4a). Consistent with the mapping and sequence analysis earlier (Fig. 2), the B'-docking SLiM in PME-1 occupies the substrate-binding groove similar to the substrate peptide from BubR1 (Fig. 4a). Five residues (V251, E252, I254, I255, and E256) in this SLiM form sidechain interactions with the B'g1 groove (Fig. 4b, interface I). Next to this B' groove features a network of salt-bridge and H-bond interactions between the PME-1 core (residues N192, Q195, N196, and R199) and B'g1 (residues D180, K183, E226, and Q266), centered at the R199-E226 salt bridge interaction (Fig. 4c, interface II). Interface III is two HEAT repeats away from interface I and involves both the PME-1 structured core and the N-terminal disordered region (1-40) (Figs. 4a&d). This interface harobrs three widely separated salt bridge interactions between PME-1 residues K217, R39, and R37, and B'g1 residues D313, E353, and E399 (Fig. 4d). The rest of the N-terminal disordered region (1-36) is invisible in the electron density map, but our earlier mapping of PME-1 disordered regions suggested that PME-1 N-terminal residues 1-18 also contribute to B'g1 interaction (Fig. 2), indicating the presence of a fourth interface. The mode of PME-1 binding is likely common for all B' subunits as the PME-1-B'g1 interface involves predominantly the B' common core (Extended Data Fig. 1a).

To assess the function of the B'-PME-1 interfaces, we introduced mutations to PME-1 and B'g1 residues at the above three interfaces. Using *in vitro* pulldown assay, we showed that all single or combined interface mutations in either PME-1 or B'g1 weakened their interactions (Figs. 4e-f), underlying that all three interfaces are essential. PME-1 mutations from each individual interface all reduced PME-1 binding to the PP2A-B'□ holoenzyme, another B' family member, and the combined mutations from three interfaces (3MU) completely disrupted this binding (Fig. 4g). These results demonstrate that B'-PME-1 interfaces are crucial for PME-1 interaction with all PP2A-B' holoenzymes, consistent with the earlier data that detects interactions between the recombinant PME-1 and multiple B' subunits in mammalian cells (Fig. 1d).

Effects of PME-1 mutations and inhibitor on different PME-1 activities

We reason that B'-PME-1 interfaces specifically dictate PME-1's activity toward PP2A-B' holoenzymes, but not the core enzyme. Consistent with this notion, PME-1 bearing 3MU above exhibits a drastically reduced methylesterase activity toward the PP2A-B'g1 holoenezyme, but an unaltered activity toward the core enzyme (Fig. 5a). In constrast, ABL127, a compound that blocks PME-1's activity by producing an

enzyme-inhibitor adduct at the PME-1 active site[35], is expected to block PME-1's activity toward all PP2A complexes. Consistent with this notion, ABL127 reduced PME-1 binding to both the core enzyme and the PP2A-B'δ holoenzyme (Fig. 5b). This result also indicates that methylesterase activation and the entry of PP2Ac tail into the PME-1 active site is essential for PME-1-holoenzyme interactions. Consistently, the cryo-EM electron density map for the PP2Ac tail is barely retained at the A-B'g1 interface, sharply different from the holoenzyme (Fig. 5c).

Our structural and biochemical observations collectively arrive at a "latch-to-induce-and-lock" model for PME-1 interaction with holoenzymes and methylesterase activation (Fig. 5d). Initial latching of PME-1 disordered regions triggers holoenzyme conformational changes, allowing PME-1 to make dual contacts to the PP2Ac active site and tail. These contacts lock a stable interaction and activate the methylesterase activity toward holoenzymes.

Uncovering and dissecting cellular PME-1 funtions in AKT-p53 signaling

The fact that PME-1 mutations at B' interfaces selectively block its function toward the PP2A-B' holoenzymes and PME-1 inhibitor blocks all PME-1 activities provides us an opportunity to dissect multi-faceted PME-1 functions in mammalian cells. PME-1 knockdown was shown to decrease PP2Ac methylation, reduce the phosphorylation level of AKT and ERK in cancer cells, and elevate PP2A-B' holoenzyme activity[36,37]. Here we show that overexpression of PME-1-mRuby fusion protein elevates the level of AKT phosphorylation at Ser473, and ABL127 significantly suppresses this elevation (Figs. 6a-b). PME-1 with 3MU or DIL suppresses this elevation similar to ABL127 (Figs. 6a-b). In contrast, ABL127 reduces the cellular level of unmethylated PP2Ac much more than those PME-1 mutants (Figs 6a-b). These data indicate that the role of PME-1 on AKT phosphorylation is mediated by its activity toward PP2A-B' holoenzymes, and B'-interface mutations selectively affect the demethylation of PP2A-B' holoenzymes, unlike ABL127 that affects the demethylation of all PP2A complexes.

p53 is a tumor suppressor and functions by inducing cell cycle arrest and apoptosis in response to DNA damage. PP2A facilitates p53 activation by targeting pThr55, inhibitory phosphorylation added by TAF1 kinase that reduces p53 stabilization[38,39]. PP2A also regulates MDM2 phosphorylation and affects its E3 ligase activity toward p53[40,41]. Furthermore, AKT facilitates p53 degradation by elevating the activity of MDM2[41,42]. The complex roles of PP2A holoenzymes in this intricate signaling network led us to dissect the versatile PME-1 functions in p53 signaling. Overexpression of PME-1-mRuby elevates p53 phosphorylation at Thr55, and ABL127 reduces this elevation (Figs. 6a-b). B'-interface mutations, 3MU and DIL, abolish this PME-1 activity comparable to or better than ABL127 (Figs. 6a-b). These data demonstrate a novel role of PME-1 in regulating p53 phosphorylation and pinpoint this cellular function to its activity toward PP2A-B' holoenzymes. Consistently, a previous study showed that p53 pThr55 is a target site of PP2A-B' holoenzymes[38].

Next, we further demonstrated the role of PME-1 in p53 signaling during DNA damage response (DDR). Upon doxorubicin treatment to induce DDR, both total p53 protein and pThr55 were increased over time

and accumulated to high levels after 24 in 293T cells (Figs. 6c-d). During DDR, the presence of ABL127 leads to a more rapid p53 accumulation, accompanied by an attenuated increase in pThr55 (Figs. 6c-d). PME-1 B'-interface mutations gave similar effects during DDR with PME-1-mRuby overexpression. PME-1 3MU leads to more rapid p53 accumulation and attenuated increase in pThr55 compared to WT PME-1 (Figs. 6e-f). These results underscore an inverse relationship between pThr55 and p53 stability and a role of PME-1 in suppressing p53 accumulation by enhancing pThr55 during DDR, and suggest that PME-1 activity toward PP2A-B' holoenzymes might contribute to this cellular function.

In summary, we demonstrated coherent roles of PME-1 in stimulating oncogenic AKT signaling and inhibiting tumor suppressor p53 signaling by enhancing activation pS473 of AKT and inhibitory pThr55 of p53. Consistent with these observations, PME-1 amplification is found in many type of cancer and associated with poorer survival outcome (Extended Data Fig. 4). The B'-interface mutations allow us to pinpoint these PME-1 functions to its activity toward PP2A-B' holoenzymes at both basal conditions and in reponse to DNA damage (Fig. 6g), suggesting a better strategy to target PME-1 than the active site inhibitor.

Discussion

Our studies reveal remarkable structural malleability and functional versatility of PME-1 for both diverse PP2A holoenzymes and complex cellular signaling. Since our first observation on PME-1-PP2A holoenzyme interactions, it has been more than a decade to gain the current level of insights into the structural, biochemical, and cellular mechanisms of PME-1 toward PP2A holoenzymes. This advance is greatly facilitated by accumulated knowledge on PP2A holoenzyme biogenesis and substrate recognition, and in turn, raises more questions and is expected to facilitate further understanding of PP2A homeostasis, substrate recognition, and complex PP2A regulations in cellular signaling.

PME-1-mediated holoenzyme demethylation would remove the methylation mark that protects PP2A holoenzymes from disassembly by a4 and TIPRL[34] and provides a mechasnim to prime PP2A holoenzymes for disassembly (Extended Data Fig. 5). *In vitro* dissection of PP2A regulation complexes arrives at a strictly controlled linear pathway for PP2A holoenzyme biogenesis: 1) stabilization of the partially-folded, latent PP2Ac by α4[33]; 2) PP2Ac activation by phosphatase activator (PTPA)[43]; 3) methylation of the active core enzyme by LCMT-1[24], and 4) methylation-facilitated formation of stable holoenzymes in cells[17,18]. Together with this pathway, holoenzyme demethylation and disassembly would form a regulation loop for holoenzyme biogenesis and recycling (Extended Data Fig. 5), which provides a tantalizing mechanism for up- and down-regulation of PP2A holoenzymes in cellular signaling. Periodic PP2A demethylation occurs during cell cycle[44], suggesting that PP2A holoenzymes might undergo cell cycle-dependent disassembly. PP2A recycling might also occur during stress or DDR, creating a window of reduced PP2A holoenzyme activity to propagate DDR signaling cascades[45]. The ability to probe holoenzyme reshuffling and in-depth understanding of PP2A holoenzyme function and

substrate recognition in related cellular signaling would be crucial to investigate such dynamic holoenzyme homeostasis in cells.

The versatile PME-1 functions toward the PP2A core enzyme and diverse holoenzymes contrast the strictly controlled LCMT-1 activity toward the active core enzyme and likely explains its more restricted cellular level and cellular location than LCMT-1. While LCMT-1 is highly abundant in cells under normal conditions[24], elevated PME-1 level is associated with many types of cancer[46,47] and neurological disorders[22,48,49]. Furthermore, PME-1 is predominantly in nucleus under normal cellular conditions[44]. These observations hint that PME-1-medated holoenzyme inhibition and decommissioning might be more regulated and restricted than LCMT-1-mediated robust holoenzyme biogenesis. How PME-1 activities are regulated and the function of its broad covalent modifications (http://phosphosite.org) remain to be investigated.

The cryo-EM structure of the PP2A-B' holoenzyme-PME-1 complex reveals remarkable structural malleability of both the holoenzyme and PME-1 (Fig. 3). This observation reinforces the dynamic nature of PP2A regulation, despite that PP2A holoenzymes are themal dynamically the most stable forms with nanomolar intersubunit binding affinities[29]. The structural dynamic not only accommodates the unexpected binding, but is also crucial for methylesterase activation. At least six separate contacts between PME-1 and PP2A-B' holoenzymes are made by both structured cores and disordered regions (Figs. 2-4). These contacts involve multiple functionally important sites, including the PME-1 active site, the phosphatase active site, and the B' substrate-binding groove, providing coherent structural basis for holoenzyme demethylation and for suppressing PP2A holoenzyme activity. The PME-1 disordered motifs synthesize novel activities by three mechanisms: tethering holoenzymes, enabling large structural shifts, and blocking holoenzyme-substrate recognition. Such structural and functional intricacy is likely a common theme for PME-1 interactions with other families of PP2A holoenzymes.

Our study provides a foundation for and demonstrate how *in vitro* structural and biochemical studies guide cellular dissetion of complex PME-1 activities. Both holoenzyme-substrate and holoenzyme-PME-1 interactions are highly dynamic and flimsy in cells, making cellular investigation extremely challenging. Taking advantage of distinct effects of PME-1 inhibitor and B' interface mutations, we pinpoint the function of PME-1 on AKT phosphorylation to its activity toward PP2A-B' holoenzymes (Fig. 5-6). This result extends the previous observation that PME-1 knockdown increased PP2A methylation, elevates PP2A-B' holoenzyme activity, and reduces AKT and ERK phosphorylation in cancer cells[36,37]. Built on the previous observation that p53 pThr55 is a target site of PP2A-B' holoenzymes[38], we demonstrated a novel cellular PME-1 function in regulating p53 pThr55 and total protein level both at basal conditions and during DDR, and that the PME-1 activity toward PP2A-B' holoenzymes contributes to this function (Fig. 6). The cellular function of PP2A holoenzymes and PME-1 in p53 signaling are expected to be more complex than outlined here (Fig. 6g). For example, AKT phosphorylates MDM2 Ser166, which enchances MDM2-p53 interaction and p53 degradation[41], and PP2A dephosphorylates this MDM2 site[40]. Further cellular dissection would rely on mechanistic understanding of PME-1 activities to and substrate

recognition by other holoenzymes, which would also facilitate targeting PME-1 in cancer and neurological disorders.

SLiMs is extremely powerful in synthesizing regulation nodes and signaling networks as demonstrated for the PPP family of phosphatases, such as SLiMs in calcineurin substrates[50] and PP4 (protein phosphatase 4) substrates[51]. Substrate SLiMs for PP2A-B' holoenzymes and PP1 (protein phosphatase 1) orchestrate sequential events regulated by PP2A holoenzymes, PP1, and kinases for precise control of cell cycle progression[52-54]. Our studies demonstrate that the combination of dynamic sets of structured cores and SLiMs creates more versatile activities in cellular signaling. Such combination might be a common theme for PP2A and other cellular signaling complexes. Efforts along this line would build our ability to overcome major challenges in deciphering dynamic PP2A functions and regulations in broad cellular processes.

Materials And Methods

Protein preparation

All protein constructs were generated by standard PCR molecular cloning strategy. PME-1 and its mutants were cloned into pQlink vector (Addgene, Cambridge, MA, USA), and proteins were overexpressed in E. coli DH5α at 23 ^{o}C overnight. The PP2A Aα and CFP-Aα (9-589)-TC were overexpressed in E. coli DH5α at 23 ^{o}C overnight[30,55]. B'γ1, B'□, and B'γ1 mutants were overexpressed at 23 ^{o}C in E. coli BL21(DE3) overnight. LCMT-1 was overexpressed at 37 ^{o}C for 4 hours in E. coli BL21(DE3)[24]. PP2Ac was overexpressed in insect cells using Bac-to-Bac baculovirus expression system[24,56]. The supernatant of cell lysate was purified over Glutathione-Sepharose 4B (GS4B) (GE Healthcare, Boston, MA, USA) or Ni-NTA resin (Qiagen). After affinity purification, all tags were cleaved by TEV, thrombin or PreScission protease and proteins were further purified by ion exchange chromatography (Source 15Q, GE Healthcare) and gel filtration chromatography (Superdex 200, GE Healthcare). GST-tagged SYT16 peptide was cloned to pQlink vector, overexpressed in E. coli DH5α, and purified over GS4B resin and ion exchange chromatography. PP2A core enzyme was assembled as previously described [30,55].

In vitro characterization and biochemical assays

FRET assay, methylation, methylesterase activity assay, co-migration over gel filtration chromatography, isothermal titration calorimetry (ITC), GST-mediated pulldown assay and binding competition, proteomic peptide phage display (Pro-PD) were described in supplemental materials.

Cryo-EM sample preparation and data acquisition

The PP2A core enzyme was assembled as described[55] and then methylated by LCMT1 in the presence of S-adenosyl methionine (SAM). The methylated PP2A core enzyme was incubated with an excess amount of B'γ1 and PME-1 containing an inactive mutation (S156A). The PP2A-PME-1 complex was purified to

homogeneity by gel-filtration chromatography. Purified PP2A-PME-1 complex was crosslinked by incubating with 0.05% glutaraldehyde for 15 min at RT and then quenched with 0.1 M Tris (pH 8.0). The crosslinked PP2A-PME-1 complex was futher purified by gel-filtration chromatography and concentrated to 1 mg/ml. For cryo-sample preparation, 3 µl of purified PP2A-PME-1 complex was applied onto a glow-discharged holey carbon grid (Quantifoil 300 mesh R 1.2/1/3 with ultrathin carbon) Grid was immediately blotted for 4 s with a blot force of 0 and plunge frozen in liquid ethane using Vitrobot (Thermo Fisher Scientific) at 4 ^{o}C and 100% humidity. Cryo-EM data was collected using a Titan Krios operating at 300 kV with a Gatan K3 detector and GIF Quantum energy filter. Movie stacks were collected using SerialEM, with a slit width of 20 eV on the energy filter and a defocus range from -1.5 µm to -2.3 µm in super-resolution counting mode at a magnification of 81,000×, corresponding to a physical pixel size of 1.059. Each stack was exposed for 3.2 s with an exposure time of 0.05 s per frame, resulting in a total of 64 frames per stack. The total dose rate was 50.8 e-/Å^2 for each stack.

Cryo-EM data processing

Movie frames were aligned using the Motioncorr2[57]. CTF parameters were estimated from the aligned micrographs using CTFFIND4[58]. Automated particle picking first using 1,000 images, particle extraction with a box size of 480 pixels, and two-dimensional (2D) classification were performed in cryoSPARC[59]. High-quality 2D class averages representing projections in different orientations were selected as templates for automatic particle picking of the entire dataset. Three rounds of 2D classification yielded 801,656 particle images with clear features of the PP2A-PME-1 complex. After ab initio model building, 3D classification into three classes with 2 reiterations to remove bad particles were performed using cryoSPARC heterogeneous refinement, followed by cryoSPARC homogenous refinement for the best class. Local refinement yielded an improved map with better details at a resolution of 3.4 Å. The resolution was estimated by applying a soft mask around the protein complex and using the gold-standard Fourier shell correlation (FSC) = 0.143 criterion.

Model building and refinement

The initial model of the PP2A-PME-1 complex was built in Pymol based on the structure of PP2A-B' holoenzyme (PDB ID: 2NPP) and PME-1-PP2A core enzyme (PDB ID : 3C5W), and manually docked into the 3.4 Å map in Chimera and adjusted in COOT[60], The structural model was refined using the phenix.real_space_refine program in PHENIX[61] with secondary structure and geometry restraints. Model was analyzed using MolProbity[62].

Mammalian cell culture and co-immunoprecipitation

Human embryonic kidney cells (HEK293T) cells were cultured in Dulbecco's modified Eagle's medium (Gibco, Thermo Fisher Scientific, Waltham, MA, USA) with 10% fetal bovine serum (Hyclone, GE Healthcare, Boston, MA, USA), 100 U/ml penicillin, and 100 µg/ml streptomycin in a humidified atmosphere at 37 °C with 5% CO2.

The HA-tagged human B' family and mRubby-tagged human PME-1were cloned into murine retroviral vectors bearing a cytomegalovirus promoter. After co-transfected into 293T cells and cultured by similar procedures mentioned above. The transfection and overexpression efficiency of B’ subunit and PME-1 were monitored by western blot using antibodies that specifically recognize HA-tag (Sigma, 12CA5, 1:1000) and PME-1(Abcam, ab86409, 1:1000). The interaction between B’ subunits and PME-1 were recognized by co-immunoprecipitation using anti-HA antibody immobilized on protein G magnetic beads (Invitrogen) before immunoprecipitate PME-1 48 h after transfection. Cells were lysed in lysis buffer (50 mM Tris-HCl pH 8.0, 150 mM NaCl, 1 mM EDTA, 1 mM Dithiothreitol and 0.5% Triton X-100) and 500 μg of cell extracts were immunoprecipitated at 4 °C in lysis buffer for 2 hours followed by western blot. A unit of 50 μg of whole-cell extracts were examined by western blot to examine the protein expression. The experiments were repeated three times and the representative results were shown.

Immunoblotting

HEK293T cells were treated with Doxorubicin (Dox) (2 μg/mL) along with ABL127 (1μM) or DMSO after the confluency reached 75%. Or HEK293T cells were transfected with different PME-1 plasmids using Lipofectamine 2000 (11668019, Thermo Fisher) and the cells were treated with Dox (2 μg/mL) to induce DNA damage for 24 h after 48 h transfection. For immunoblotting, samples were collected and suspended in ice-cold RIPA lysis buffer containing 150 mM NaCl, 0.1% Triton X-100, 0.5% sodium deoxycholate, 0.1% SDS, 50 mM Tris-HCl pH 8.0, protease inhibitor cocktail (11836170001, Sigma Aldrich) and phosphatase inhibitor cocktail (4906845001, Sigma Aldrich) at indicated time. The lysates were centrifuged at 13,000 g for 20 min at 4 ^{o}C and the supernatant was collected. The whole protein (30 μg) was analyzed by 12% SDS-PAGE followed by Western blot. The total protein and phosphorylation of p53 at Thr55 and p53 total protein were detected by anti-p53 antibody (Cell signaling, 1C12, 1:1000) and anti-p53 pThr55 antibody (Abcam, ab183546, 1:1000). The experiments were repeated three times and the representative results were shown.

Declarations

Author Contributions

YL performed biochemical, cryo-EM, and cell biology studies. MR, CW, and YX assisted the biochemical and cryo-EM studies. APB, YI, and SS contributed to cell biology, Pro-PD, and cellular PME-1-PP2A holoenzyme interactions, respectively. YL processed cryo-EM data and determined the structure. YX guided all the studies and wrote the manuscript, assisted by YL.

Acknowledgement

We thank Drs Janette Myers and Irina V Novikova from PNCC (Pacific Northwest Cryo-EM Center) for assistance and discussions on cryo-EM data collection and processing, and Kenneth Satyshur and Ivan Andrewjeski from School of Medicine for IT support. We thank Drs Robert Kirchdoerfer and Elizabeth Wright from UW-Madison and Ning Yan from Princeton University for discussions on cryo-EM studies.

References

1. Arnold, H.K. & Sears, R.C. A tumor suppressor role for PP2A-B56α through negative regulation of c-Myc and other key oncoproteins. *Cancer and Metastasis Reviews* **27**, 147-158 (2008).
2. Wlodarchak, N. & Xing, Y. PP2A as a master regulator of the cell cycle. *Critical reviews in biochemistry and molecular biology* **51**, 162-184 (2016).
3. Virshup, D.M. Protein phosphatase 2A: a panoply of enzymes. *Current opinion in cell biology* **12**, 180-185 (2000).
4. Strack, S. et al. Protein Phosphatase 2A Holoenzyme Assembly: IDENTIFICATION OF CONTACTS BETWEEN B-FAMILY REGULATORY AND SCAFFOLDING A SUBUNITS. **277**, 20750-20755 (2002).
5. Saraf, A., Oberg, E.A. & Strack, S. Molecular determinants for PP2A substrate specificity: charged residues mediate dephosphorylation of tyrosine hydroxylase by the PP2A/B' regulatory subunit. *Biochemistry* **49**, 986-995 (2010).
6. Shi, Y. Serine/threonine phosphatases: mechanism through structure. *Cell* **139**, 468-484 (2009).
7. Eichhorn, P.J.A., Creyghton, M.P. & Bernards, R. Protein phosphatase 2A regulatory subunits and cancer. *Biochimica et Biophysica Acta (BBA)-Reviews on Cancer* **1795**, 1-15 (2009).
8. Li, X. & Virshup, D.M. Two conserved domains in regulatory B subunits mediate binding to the A subunit of protein phosphatase 2A. *European journal of biochemistry* **269**, 546-552 (2002).
9. Slupe, A.M., Merrill, R.A. & Strack, S. Determinants for Substrate Specificity of Protein Phosphatase 2A %J Enzyme Research. **2011**, 8 (2011).
10. Wu, C.-G. et al. PP2A-B' holoenzyme substrate recognition, regulation and role in cytokinesis. *Cell discovery* **3**, 17027 (2017).
11. Hertz, E.P.T. et al. A conserved motif provides binding specificity to the PP2A-B56 phosphatase. *Molecular cell* **63**, 686-695 (2016).
12. Wang, J. et al. Crystal structure of a PP2A B56-BubR1 complex and its implications for PP2A substrate recruitment and localization. *Protein & cell* **7**, 516-526 (2016).
13. Wang, X., Bajaj, R., Bollen, M., Peti, W. & Page, R.J.S. Expanding the PP2A interactome by defining a B56-specific SLiM. **24**, 2174-2181 (2016).
14. De Baere, I. et al. Purification of porcine brain protein phosphatase 2A leucine carboxyl methyltransferase and cloning of the human homologue. *Biochemistry* **38**, 16539-16547 (1999).
15. Lee, J. & Stock, J. Protein phosphatase 2A catalytic subunit is methyl-esterified at its carboxyl terminus by a novel methyltransferase. *Journal of Biological Chemistry* **268**, 19192-19195 (1993).
16. Lee, J., Chen, Y., Tolstykh, T. & Stock, J. A specific protein carboxyl methylesterase that demethylates phosphoprotein phosphatase 2A in bovine brain. *Proceedings of the National Academy of Sciences* **93**, 6043-6047 (1996).
17. Bryant, J.C., Westphal, R.S. & Wadzinski, B.E. Methylated C-terminal leucine residue of PP2A catalytic subunit is important for binding of regulatory Bα subunit. *Biochemical Journal* **339**, 241-246 (1999).

18. Tolstykh, T., Lee, J., Vafai, S. & Stock, J.B. Carboxyl methylation regulates phosphoprotein phosphatase 2A by controlling the association of regulatory B subunits. *The EMBO journal* **19**, 5682-5691 (2000).
19. Janssens, V., Goris, J. & Van Hoof, C. PP2A: the expected tumor suppressor. *Current opinion in genetics & development* **15**, 34-41 (2005).
20. Sontag, E. et al. Downregulation of protein phosphatase 2A carboxyl methylation and methyltransferase may contribute to Alzheimer disease pathogenesis. *Journal of Neuropathology & Experimental Neurology* **63**, 1080-1091 (2004).
21. Lee, J.A. & Pallas, D.C.J.J.o.B.C. Leucine carboxyl methyltransferase-1 is necessary for normal progression through mitosis in mammalian cells. **282**, 30974-30984 (2007).
22. Ortega-Gutierrez, S., Leung, D., Ficarro, S., Peters, E.C. & Cravatt, B.F.J.P.o. Targeted disruption of the PME-1 gene causes loss of demethylated PP2A and perinatal lethality in mice. **3**, e2486 (2008).
23. Xing, Y. et al. Structural mechanism of demethylation and inactivation of protein phosphatase 2A. *Cell* **133**, 154-163 (2008).
24. Stanevich, V. et al. The structural basis for tight control of PP2A methylation and function by LCMT-1. *Molecular cell* **41**, 331-342 (2011).
25. Xie, H. & Clarke, S. Protein phosphatase 2A is reversibly modified by methyl esterification at its C-terminal leucine residue in bovine brain. *Journal of Biological Chemistry* **269**, 1981-1984 (1994).
26. Stanevich, V. et al. Mechanisms of the scaffold subunit in facilitating protein phosphatase 2A methylation. *PloS one* **9**, e86955 (2014).
27. Yu, X.X. et al. Methylation of the protein phosphatase 2A catalytic subunit is essential for association of Bα regulatory subunit but not SG2NA, striatin, or polyomavirus middle tumor antigen. **12**, 185-199 (2001).
28. Wu, J. et al. Carboxyl methylation of the phosphoprotein phosphatase 2A catalytic subunit promotes its functional association with regulatory subunits in vivo. *The EMBO journal* **19**, 5672-5681 (2000).
29. Chen, Y. et al. Structural and biochemical insights into the regulation of protein phosphatase 2A by small t antigen of SV40. *Nature structural & molecular biology* **14**, 527-534 (2007).
30. Wlodarchak, N. et al. Structure of the Ca 2+-dependent PP2A heterotrimer and insights into Cdc6 dephosphorylation. *Cell research* **23**, 931 (2013).
31. Xu, Y., Chen, Y., Zhang, P., Jeffrey, P.D. & Shi, Y. Structure of a protein phosphatase 2A holoenzyme: insights into B55-mediated Tau dephosphorylation. *Molecular cell* **31**, 873-885 (2008).
32. Xu, Y. et al. Structure of the protein phosphatase 2A holoenzyme. **127**, 1239-1251 (2006).
33. Jiang, L. et al. Structural basis of protein phosphatase 2A stable latency. **4**, 1699 (2013).
34. Wu, C.-G. et al. Methylation-regulated decommissioning of multimeric PP2A complexes. **8**, 2272 (2017).
35. Bachovchin, D.A. et al. Academic cross-fertilization by public screening yields a remarkable class of protein phosphatase methylesterase-1 inhibitors. *Proceedings of the National Academy of Sciences*

108, 6811-6816 (2011).

36. Puustinen, P. et al. PME-1 protects extracellular signal-regulated kinase pathway activity from protein phosphatase 2A–mediated inactivation in human malignant glioma. *Cancer research* **69**, 2870-2877 (2009).
37. Li, J. et al. Genetic amplification of PPME1 in gastric and lung cancer and its potential as a novel therapeutic target. **15**, 128-134 (2014).
38. Li, H.H., Cai, X., Shouse, G.P., Piluso, L.G. & Liu, X. A specific PP2A regulatory subunit, B56γ, mediates DNA damage-induced dephosphorylation of p53 at Thr55. *The EMBO journal* **26**, 402-411 (2007).
39. Wu, Y. et al. Phosphorylation of p53 by TAF1 inactivates p53-dependent transcription in the DNA damage response. *Molecular cell* **53**, 63-74 (2014).
40. Okamoto, K. et al. Cyclin G recruits PP2A to dephosphorylate Mdm2. *Molecular cell* **9**, 761-771 (2002).
41. Malmlöf, M., Roudier, E., Högberg, J. & Stenius, U. MEK-ERK-mediated phosphorylation of Mdm2 at Ser-166 in hepatocytes Mdm2 is activated in response to inhibited Akt signaling. *Journal of Biological Chemistry* **282**, 2288-2296 (2007).
42. Ogawara, Y. et al. Akt enhances Mdm2-mediated ubiquitination and degradation of p53. *Journal of Biological Chemistry* **277**, 21843-21850 (2002).
43. Guo, F. et al. Structural basis of PP2A activation by PTPA, an ATP-dependent activation chaperone. *Cell research* **24**, 190 (2014).
44. Longin, S. et al. Spatial control of protein phosphatase 2A (de) methylation. *Experimental cell research* **314**, 68-81 (2008).
45. Kong, M., Ditsworth, D., Lindsten, T. & Thompson, C.B. α4 is an essential regulator of PP2A phosphatase activity. *Molecular cell* **36**, 51-60 (2009).
46. Kaur, A. et al. PP2A inhibitor PME-1 drives kinase inhibitor resistance in glioma cells. (2016).
47. Wandzioch, E. et al. PME-1 modulates protein phosphatase 2A activity to promote the malignant phenotype of endometrial cancer cells. *Cancer research* (2014).
48. Sontag, J.M., Nunbhakdi-Craig, V., Mitterhuber, M., Ogris, E. & Sontag, E. Regulation of protein phosphatase 2A methylation by LCMT1 and PME-1 plays a critical role in differentiation of neuroblastoma cells. *Journal of neurochemistry* **115**, 1455-1465 (2010).
49. Nicholls, R.E. et al. PP2A methylation controls sensitivity and resistance to β-amyloid–induced cognitive and electrophysiological impairments. *Proceedings of the National Academy of Sciences* **113**, 3347-3352 (2016).
50. Roy, J. & Cyert, M.S. Cracking the phosphatase code: docking interactions determine substrate specificity. *Sci. Signal.* **2**, re9-re9 (2009).
51. Ueki, Y. et al. A consensus binding motif for the PP4 protein phosphatase. *Molecular Cell* **76**, 953-964. e6 (2019).
52. Bollen, M. Cell cycle: it takes three to find the exit. *Nature* **517**, 29 (2015).

53. Hendrickx, A. et al. Docking motif-guided mapping of the interactome of protein phosphatase-1. *Chemistry & biology* **16**, 365-371 (2009).
54. Lesage, B., Qian, J. & Bollen, M. Spindle checkpoint silencing: PP1 tips the balance. *Current Biology* **21**, R898-R903 (2011).
55. Xing, Y. et al. Structure of protein phosphatase 2A core enzyme bound to tumor-inducing toxins. *Cell* **127**, 341-353 (2006).
56. Zhang, L. et al. Eya3 partners with PP2A to induce c-Myc stabilization and tumor progression. *Nature communications* **9**, 1-14 (2018).
57. Zheng, S.Q. et al. MotionCor2: anisotropic correction of beam-induced motion for improved cryo-electron microscopy. *Nature methods* **14**, 331-332 (2017).
58. Rohou, A. & Grigorieff, N. CTFFIND4: Fast and accurate defocus estimation from electron micrographs. *Journal of structural biology* **192**, 216-221 (2015).
59. Punjani, A., Rubinstein, J.L., Fleet, D.J. & Brubaker, M.A. cryoSPARC: algorithms for rapid unsupervised cryo-EM structure determination. *Nature methods* **14**, 290-296 (2017).
60. Emsley, P., Lohkamp, B., Scott, W.G. & Cowtan, K. Features and development of Coot. *Acta Crystallographica Section D: Biological Crystallography* **66**, 486-501 (2010).
61. Adams, P.D. et al. PHENIX: a comprehensive Python-based system for macromolecular structure solution. *Acta Crystallographica Section D: Biological Crystallography* **66**, 213-221 (2010).
62. Chen, V.B. et al. MolProbity: all-atom structure validation for macromolecular crystallography. *Acta Crystallographica Section D: Biological Crystallography* **66**, 12-21 (2010).

Figures

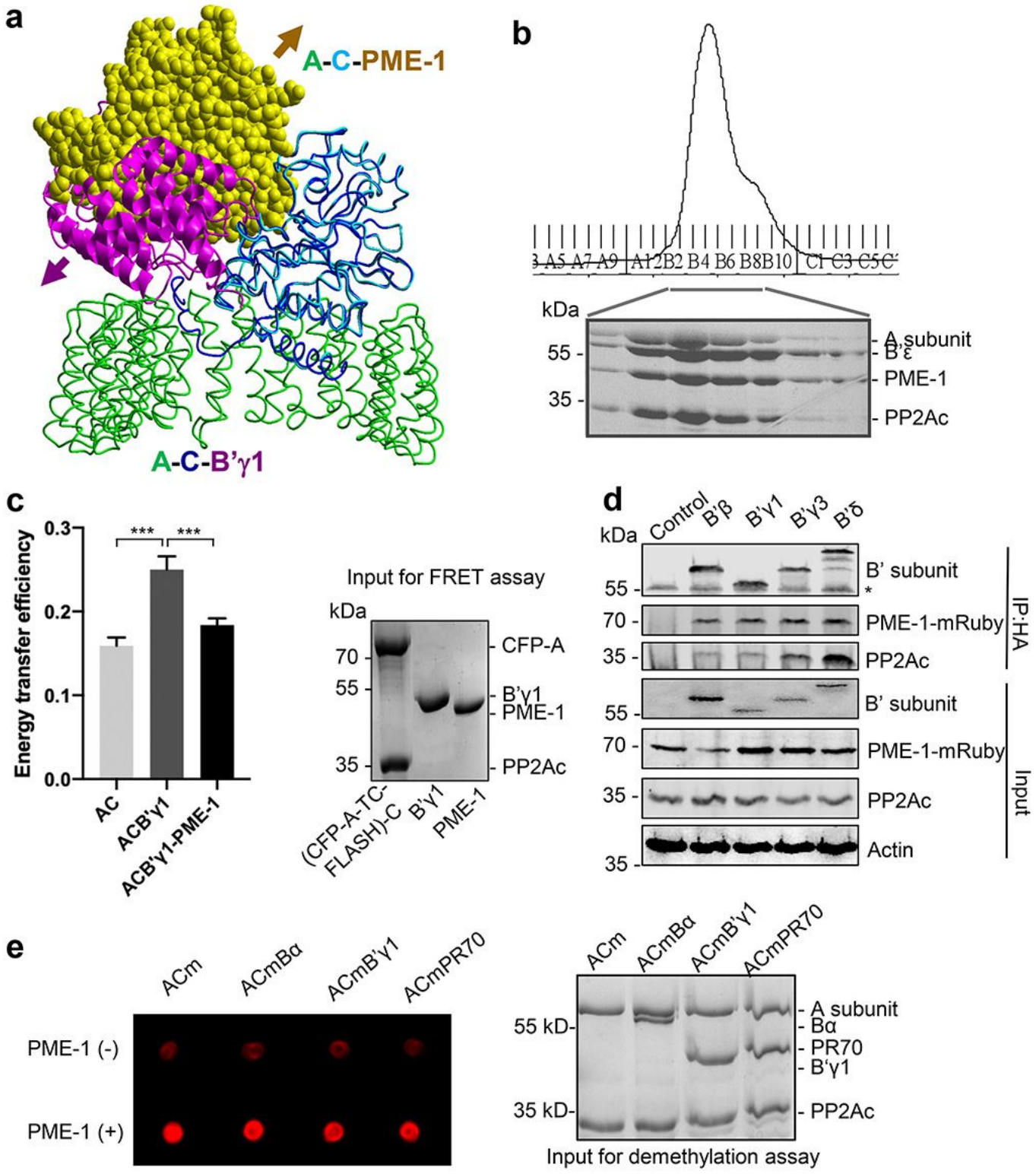

Figure 1

PME-1 directly interacts with and demethylates PP2A holoenzymes. a, Structural overlay of the PP2A-B'γ1 holoenzyme (PDB code: 2NPP) to the PP2A core enzyme-PME-1 complex (PDB code: 3C5W) aligned via PP2Ac (C) and the C-terminal five HEAT repeats of the A-subunit. It illustrates the steric hindrance of regulatory subunits to exclude PME-1 binding to the holoenzymes. b, The PP2A-B'ε holoenzyme and PME-1 co-migrate over gel filtration chromatography. Protein fractions were analyzed by SDS-PAGE and

visualized by Coomassie blue staining. c, FRET assay measured changes in the distance between the A-subunit N- and C-termini in the PP2A core enzyme prior to and after addition of B’γ1 with and without PME-1 (left). Representative results were shown with mean ± SEM calculated from three experimental repeats. Protein inputs used in FRET assay was shown (right). d, Co-immunoprecipitation (co-IP) of PME-1-mRuby and PP2Ac by HA-tagged B' (B’β, B’γ1, B’γ3, and B’δ) recombinantly expressed in HEK 293T cells. e, PME-1 catalyzes demethylation of methylated core enzyme and holoenzymes in vitro. The level of demethylation was determined by 4b7 antibody that specifically recognizes the unmethylated PP2Ac (left). Input of PP2A complexes was shown (right).

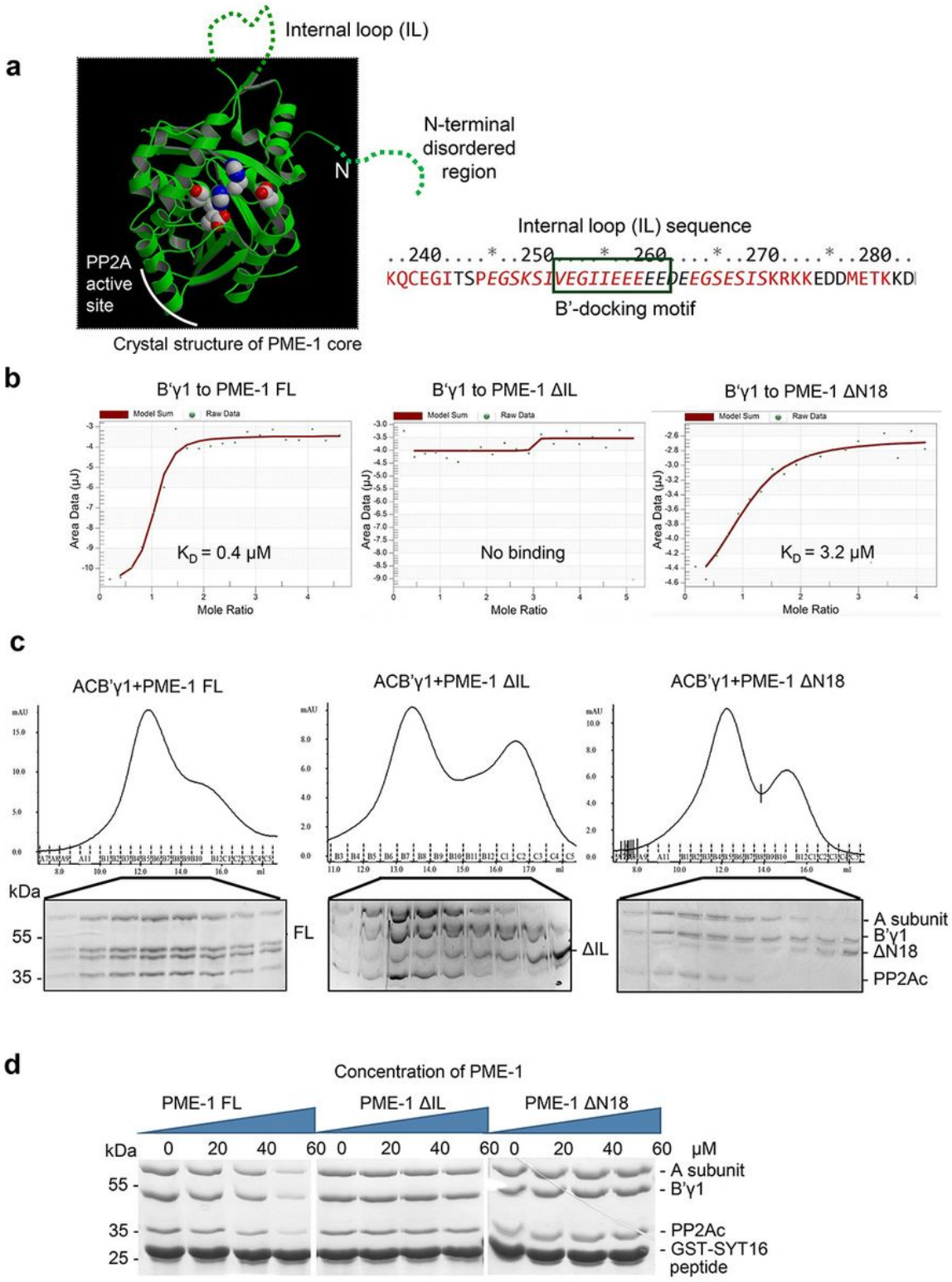

Figure 2

Mapping of PME-1 interactions with B'γ1 and the PP2A-B'γ1 holoenzyme. a, The crystal structure of the apo-PME-1 structured core (PDB code: 3C5V), with the N-terminal disordered region and internal loop shown in dashed lines (left). The internal loop sequence harbors a substrate-mimicking B'-docking motif (right). b, ITC measured binding affinities of B'γ1 to PME-1 FL and truncated mutants (ΔIL and ΔN18). c, Co-migration of the PP2A-B'γ1 holoenzyme and PME-1 and effects of ΔN18 and ΔIL. d, Pull-down of the

PP2A-B'γ1 holoenzyme via GST-tagged substrate peptide (GST-SYT16) in the present and absence of increasing concentrations of PME-1 FL, ΔN18 or ΔIL. Proteins associated with GS4B resins were examined by SDS-PAGE and visualized by Coomassie blue staining.

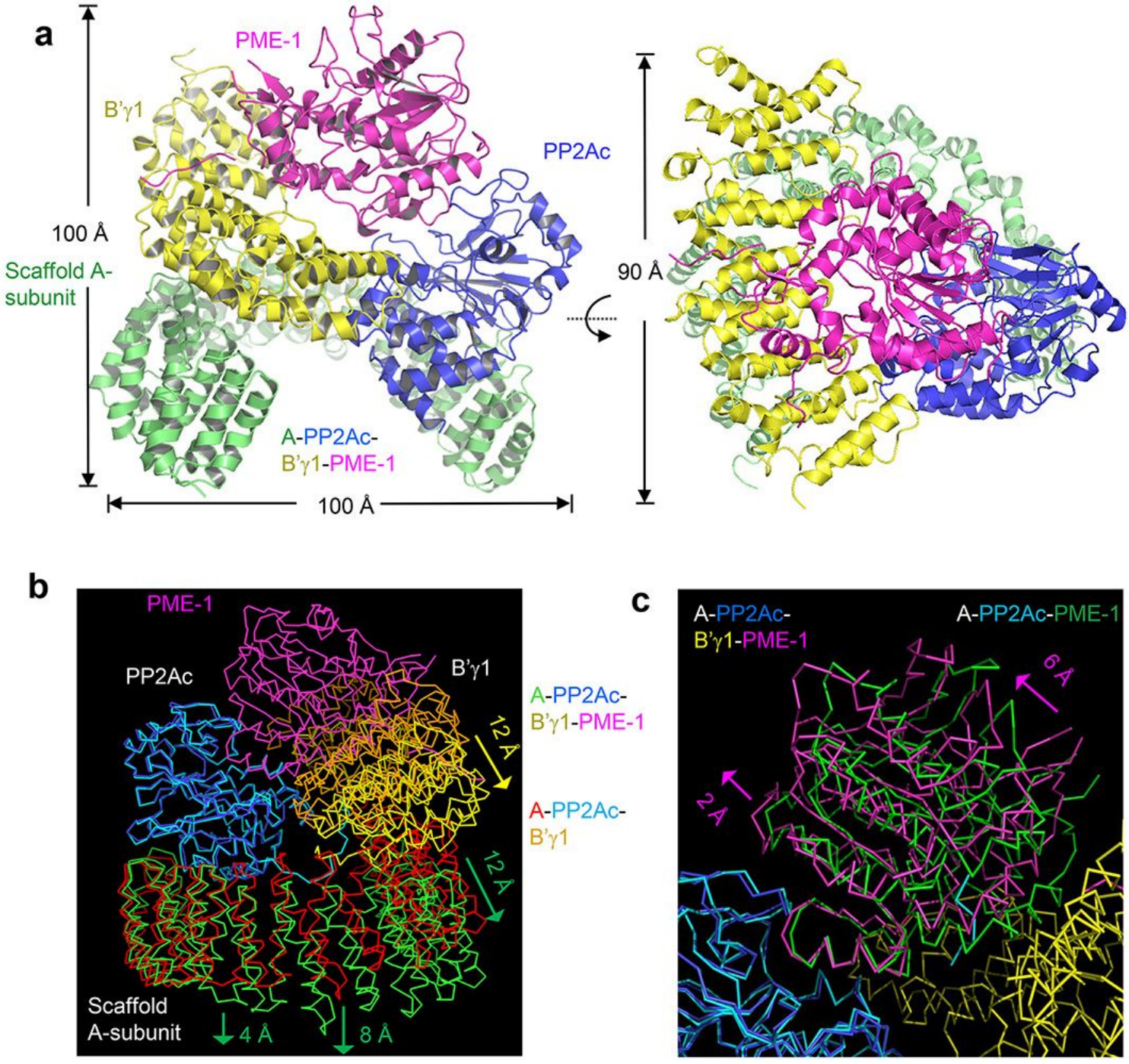

Figure 3

Cryo-EM structure of the PP2A-B'γ1-PME-1 complex. a, Overall structure of the PP2A-B'γ1-PME-1 complex. Two perpendicular views are shown. The A-subunit, PP2Ac, B'γ1, and PME-1 are shown in cartoon and colored green, blue, yellow and magenta, respectively. The structure of the PP2A-B'γ1-PME-1 complex is overlaid to the PP2A-B'γ1 holoenzyme (PDB code: 2NPP) b, and the PP2A core enzyme-PME-1 complex (PDB code: 3C5W) c, aligned via PP2Ac. For B&C, all models are shown in ribbon. The PP2A-B'γ1-PME-1

complex is colored as in b. The A-subunit, PP2Ac, and B'γ1 in the holoenzyme are colored red, cyan, and orange, respectively. PP2Ac and PME-1 in the PP2A core enzyme-PME-1 complex are colored cyan and green, respectively. See also movie s1.

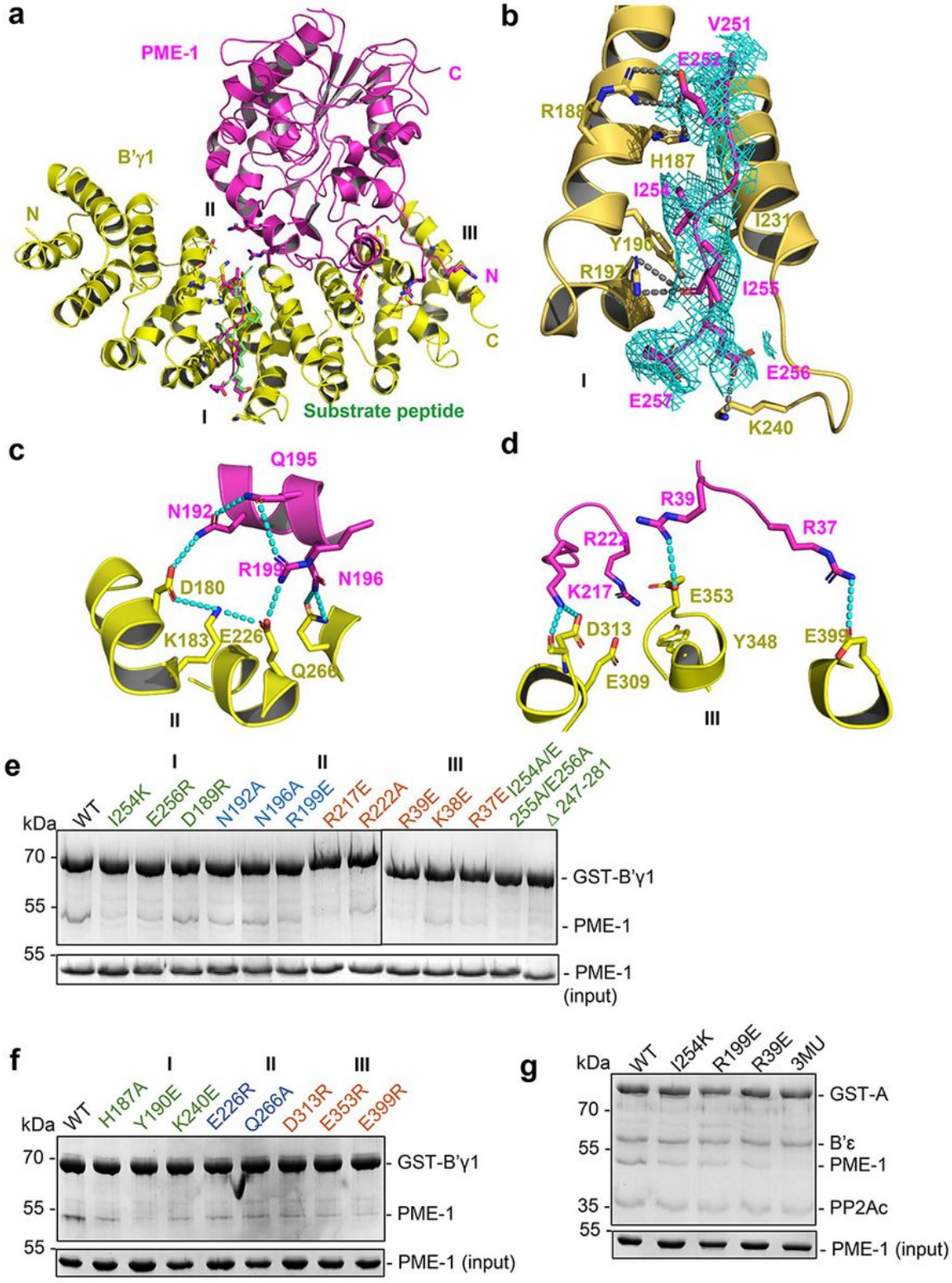

Figure 4

B'-PME-1 interfaces. a, An overview of interactions between B'γ1 (yellow) and PME-1 (magenta). The SLiM in the PME-1 internal loop was perfectly overlaid with the BubR1 subtrate peptide from the B'γ1-

BubR1 complex (PBD code: 5JJA) aligned by B'γ1. b-d, Close-up views of interaction interfaces I, II, and III between B'γ1 and PME-1. B'γ1 and PME-1 residues are shown in stick and colored yellow and magenta, respectively. The cryo-EM electron density map for the SLiM in PME-1 was colored cyan and shown at 4 Å. e-g, In vitro pull down of wild-type or mutant PME-1 proteins by GST-B'γ1 (e), GST-B'γ1 mutants (f), or GST-PP2A-B'ε holoenzyme (g).

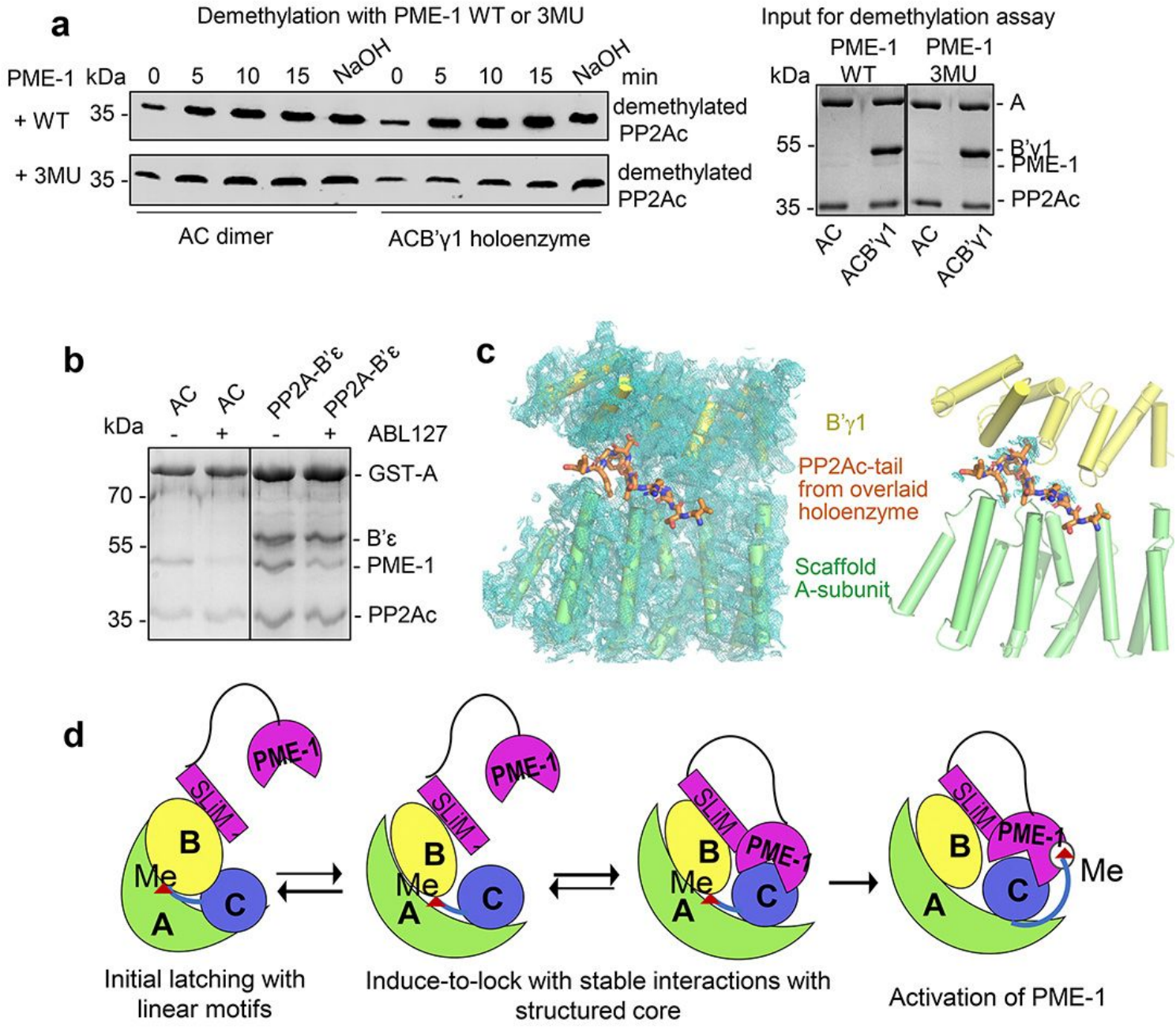

Figure 5

Different effects of PME-1 inhibitor and B'-PME-1 interface mutations. a, WT and mutant (3MU) PME-1-catalyzed demethylation of methylated core enzyme and PP2A-B'γ1 holoenzyme. The level of demethylation and protein input was determined as in Fig. 1e. b, Pulldown of wild-type PME-1 by GST-tagged PP2A core enzyme or PP2A-B'γ holoenzyme in the presence or absence of ABL127 PME-1 inhibitor. Proteins bound to GS4B resins were examined as in Fig. 2D. c, Illustration of the A-B'γ1 interface

and the PP2Ac tail from the overlaid holoenzyme with the cryo-EM map shown at 3.5 Å. The map for the A-subunit and B'γ1 (left) and the overlaid holoenzyme tail (right) are shown separately for comparison. A-subunit, B'γ1, and electron density map are colored as in Figs. 3-4. The PP2Ac tail from the overlaid holoenzyme are shown in stick and colored orange. d, The latch-to-induce-and-lock model for PME-1 interactions with and methylesterase activation toward PP2A holoenzymes. In brief, PME-1 disordered motifs, including substrate-mimicking SLiM, latch to the regulatory subunit, enabling holoenzyme conformational changes, PME-1 interactions with PP2Ac and the movement of PP2Ac tail from the holoenzyme interface to the PME-1 active site. See also movie s1.

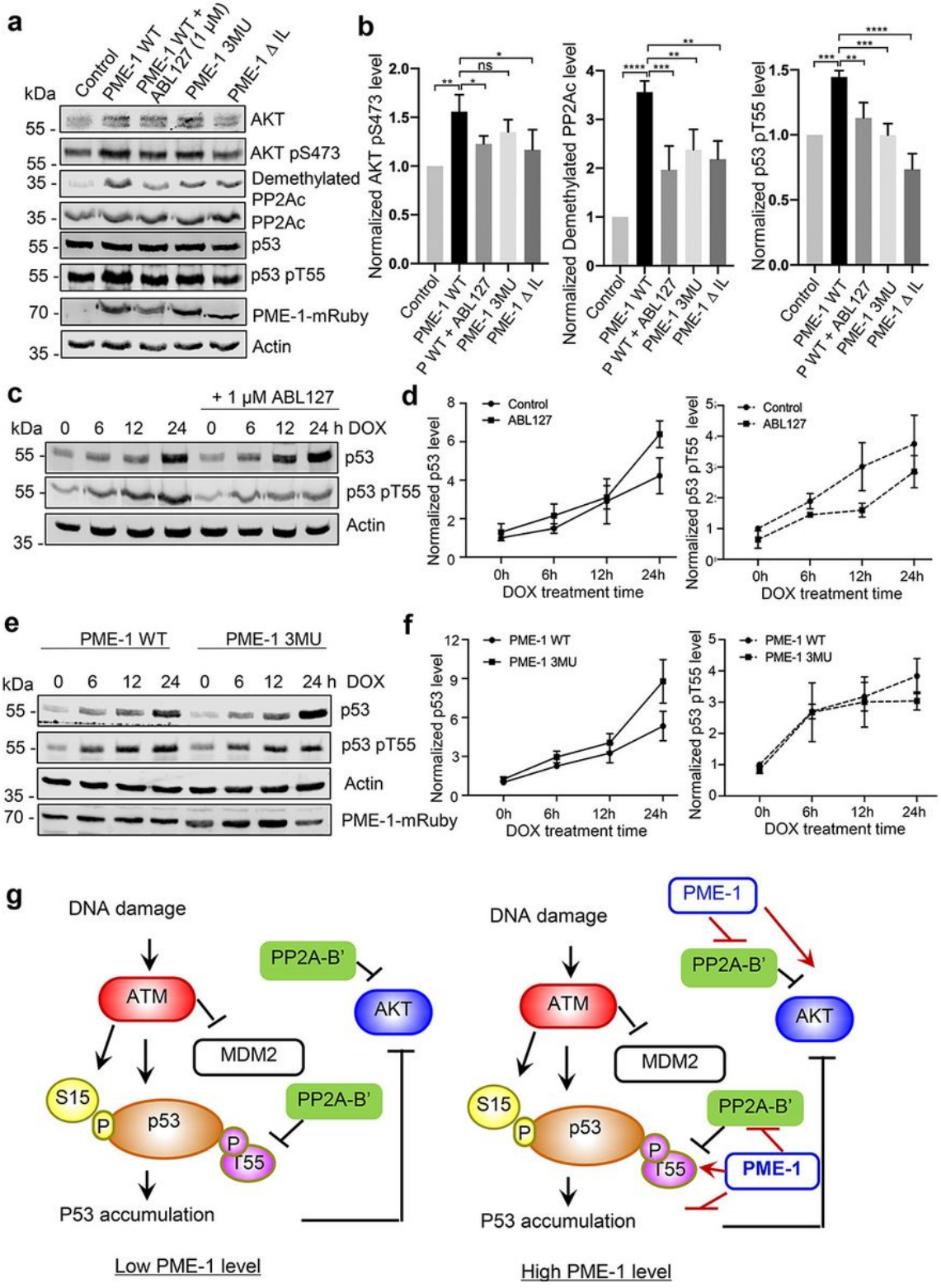

Figure 6

Cellular dissection and uncovering of PME-1 function in AKT-p53 signaling. a, Effects of PME-1 inhibitor versus B' interface mutations on AKT phosphorylation at Ser473, p53 phosphorylation at Thr55, and cellular PP2Ac methylation. The mock vector, wild-type or mutant PME-1 were transfected into 293T cells, followed by treatment by ABL127 as indicated. Total cell lysates were examined by western blot. b, Cellular levels of AKT pSer473, p53 pThr55, and demethylated PP2Ac in a were analyzed and mean ±

SEM was calculated from three experimental repeats. c, Effects of PME-1 inhibitor on p53 accumulation and phosphorylation at T55 during DDR. 293T cells were treated with DOX (2 μg/mL) in the presence of ABL127 (1μM) or DMSO for indicated time. Total p53 and pThr55 were detected at indicated time points. Time-dependent increase in p53 total protein and pThr55 were calculated from three repeats and mean ± SEM was shown. d, ABL127 attenuates the increase in pThr55 and inversely accelerates p53 accumulation. e, Effects of PME-1 mutatons at B'-interface on p53 accumulation and phosphorylation at T55 during DDR. 293T Cells were treated with DOX (2 μg/mL) after 48 h transfection with wild-type or mutant PME-1. Total p53 and pThr55 were detected at indicated time points. Time-dependent increase in p53 total protein and pThr55 was analyzed as d and shown in f. PME-1 mutations accelerates p53 accumulation with attenuated increase in pThr55. g, Illustration of AKT-p53 signaling and roles of PP2A-B' holoenzymes in suppressing AKT activity and enhancing p53 accumulation (left). PME-1 overexpression stimulates AKT activity and suppresses p53 accumulation by suppressing PP2A-B' holoenzymes (right).

Supplementary Files

This is a list of supplementary files associated with this preprint. Click to download.

- PME1manuscriptsupplemental.pdf